



Thermoluminescence assessment of quartz veins emplaced in Talc-Schist Metamorphic Rocks, Egypt

Nabil El-Faramawy^{1,a)} , Ahmed Gad², Huda A. Alazab³, Shrouk Farouk¹

¹ Physics Department, Faculty of Science, Ain Shams University, Abbassia, Cairo 11566, Egypt

² Geology Department, Faculty of Science, Ain Shams University, Abbassia, Cairo 11566, Egypt

³ Egyptian Atomic Energy Authority, 3-Ahmed El-Zomor St. El-Zohour Sect, Nasr City, Cairo 11762, Egypt

^{a)} Address all correspondence to this author. e-mail: nabil_elfaramawi1@sci.asu.edu.eg

Received: 15 May 2022; accepted: 19 September 2022; published online: 19 October 2022

The current work is aimed to study the thermoluminescence (TL) properties of natural milky quartz associated with Metamorphic Rocks extracted from the Eastern Desert of Egypt. Atomic absorption spectrometer was used to assess the chemical compositions of the samples, and X-ray diffraction was used to examine the structural properties (XRD). The deconvolution of the glow curve was carried out and revealed that there were ten trapping sites at 0.623, 0.936, 1.02, 1.06, 1.31, 1.47, 1.58, 1.76, 2.49, and 2.96 eV. The linearity of the sample was examined for each glow peak. The analysis of the glow curve was studied also by $T_m - T_{stop}$ and various heating rates (VHR) giving the kinetics parameters (activation energy E , eV). The minimum detectable dose of the investigated samples was found to be 24 μ Gy. The dosimeter demonstrated a high level of repeatability. The fading signal was investigated for varying storage times up to 30 days.

Introduction

Quartz (SiO_2) is one of the most abundant minerals in the earth's crust and it was found in a variety of geologic settings [1]. It is an important rock forming mineral in igneous, metamorphic, and sedimentary. Quartz is formed by primary and secondary magmatic, hydrothermal, or sedimentary processes or during diagenesis and metamorphosis [2]. Magmatic and post-magmatic processes may accumulate large amounts of quartz in pegmatites and hydrothermal deposits [3]. Quartz veins represent mineralization from hydrothermal fluids along various types of fault systems. Quartz can also be mobilized and crystallized during metamorphic processes (e.g., Heynke et al. [4]).

Quartz generally is formed in Egypt in the Eastern Desert in association with igneous and metamorphic rocks [5]. The pre-cambrian basement complex rocks (igneous–metamorphic) of Egypt, covering approximately $\sim 100,000 \text{ km}^2$, crops out mainly along the Red Sea Mountains range in the Eastern Desert and southern Sinai Peninsula [6–8]. These rocks comprise three main tectonostratigraphic elements: (1) infrastructural rocks consisting of schists and high-grade gneisses and migmatites, (2) arc-type volcanic/volcano-sedimentary units, along with dismembered ophiolites, and (3) the Ediacaran Hammamat and

Dkhan supracrustal sequences. Granitoids impose all the three elements [9–11].

The effects of the annealing process and irradiation on the sensitivity and superlinearity behavior of the 383 K-TL peak were studied for three types of quartz: high-purity synthetic quartz, natural Arkansas quartz of hydrothermal origin, and sedimentary quartz from the coast of the Chalkidiki region in Northern Greece by Polymeris et al. [12]. In addition, Zhou et al. [13] made their study on the kinetic analysis of natural quartz from China.

Thermoluminescence (TL) is a phenomenon in which a material (mineral) emits light while it is being heated. It is a stimulated emission process occurring when the thermally excited emission of light is followed by absorption of energy from irradiation. Absorbed energy from ionizing radiation (alpha, beta, gamma, cosmic rays) frees electrons and some of which get trapped at the crystal lattice imperfections. Both Furetta [14] and Pagonis [15] studied the successive heating of the crystal that can release some of these trapped electrons with an associated emission of light. The graph between the intensity of the emitted light with the applied heat is called glow curve [16]. This glow curve can be considered as a "fingerprint" of the mineral and it does not only depend on the nature of the

phosphors involved, but also on the dose received in nature, i.e., the period over which this dose is delivered, and the temperature(s) experienced by the specimen during this time. The TL phenomenon was exhibited by many natural minerals like calcite [17, 18], feldspars [19], fluorapatite [20], ulexite [21], and dolomite [22].

The TL glow curves have different shapes depending on the nature and origin of quartz. Murray and Wintle [23] noticed that the changes in TL sensitivity for 30,000 year old of quartz extracted from Australia. The effect of thermal treatments on the TL glow curves and the emission spectra of a natural quartz crystal were studied by De Lima et al. [24]. Kinetic analysis of the TL glow curve of quartz using the various analysis techniques was carried out by Kitis et al. [25]. In 2020, Farouk et al. [26] studied the thermoluminescence properties for quartz samples collected from the Central Eastern Desert (CED), Egypt. The same group studied also the thermoluminescence response and its kinetic analysis of natural milky quartz associated with tin-tungsten-fluorite mineralization [27].

The current work is focused on studying the dosimetric properties of a new type of Egyptian milky quartz extracted from Metamorphic Rocks.

Results and discussion

XRD results

The X-ray diffraction pattern of the sample powder is shown in Fig. 1. The diffraction peaks are observed at 20.8°, 26.9°, 26.7°, 29.37°, 36.5°, 39.5°, 40.3°, 42.4°, 45.8°, 50.1°, 54.9°, 55.3°, 59.9°, 64°, 65.7°, 67.7°, 68.1°, 68.3°, 73.5°, 73.7°, 75.6°, and 77.7°. The peak locations of the investigated samples were represented by the red lines. The obtained peaks were compared with the standard powder diffraction cards of the International Centre for diffraction data (ICDD). The diffraction peaks are matched

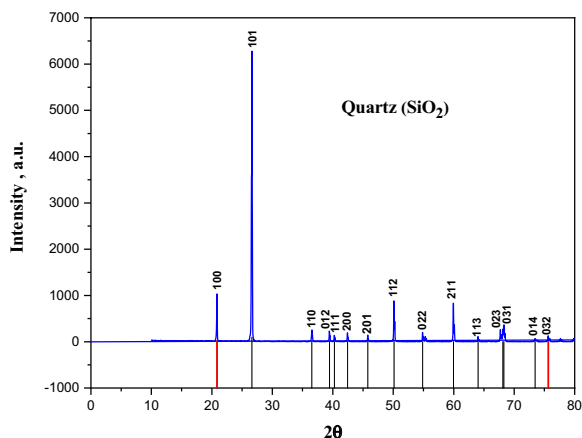


Figure 1: XRD pattern of the Egyptian milky quartz samples.

to a hexagonal quartz (ICDD card no. 03-065-0466) with lattice parameters of $a = b = 4.92 \text{ \AA}$ and $c = 17.35 \text{ \AA}$. The average crystal size was checked by scanning electron microscope (SEM) it was approximately $2 \mu\text{m}$ as shown in Fig. 2.

Elementary analysis results

The composition of element concentrations for the investigated milky quartz takes the following order of $\text{Si} (1.2 \text{ E} + 6) > \text{Ti} (1.7 \text{ E} + 5) > \text{Al} (1.2 \text{ E} + 4) > \text{Na} (76.9) > \text{Ca} (60.5) > \text{Mg} (33) > \text{Li} = \text{Mn} (1.97)$. The higher values were achieved for Si concentrations as expected due to quartz being SiO_2 mineral. The analyses of elemental concentrations revealed that the higher impurities with SiO_2 were found to be Ti and Al elements. Due to higher concentrations of Ti and Al elements, glow curves of investigated quartz samples have different shapes.

Dosimetric properties

Glow curve and dose response curve

The glow curves of the examined milky quartz were obtained after being exposed to various beta-radiation doses in a range of 0.11 Gy up to 220 Gy. The TL intensity was changed with the various applied doses (Fig. 3). The deconvoluted glow curves to six different beta doses of 0.33, 1.1, 5.5, 55, 110, and 220 Gy are shown in Fig. 4. The deconvolution was carried out on the glow curves obtaining ten overlapping thermoluminescence peaks in temperature ranging from 325 to 650 K. The ten deconvoluted peaks were located at 310.2 ± 2.9 , 373.7 ± 0.7 , 399.8 ± 1.1 , 425.3 ± 3.2 , 440.3 ± 2.3 , 463.8 ± 1.8 , 496.5 ± 6.2 , 550.6 ± 10.2 , 576.5 ± 9.8 and 622.8 ± 8.6 K. The corresponding trap energies of these TL peaks were 0.66 ± 0.03 , 0.94 ± 0.06 , 1.02 ± 0.03 , 1.06 ± 0.06 , 1.31 ± 0.04 , 1.47 ± 0.04 , 1.58 ± 0.08 , 1.75 ± 0.05 , 2.49 ± 0.15 , and 2.95 ± 0.16 eV.

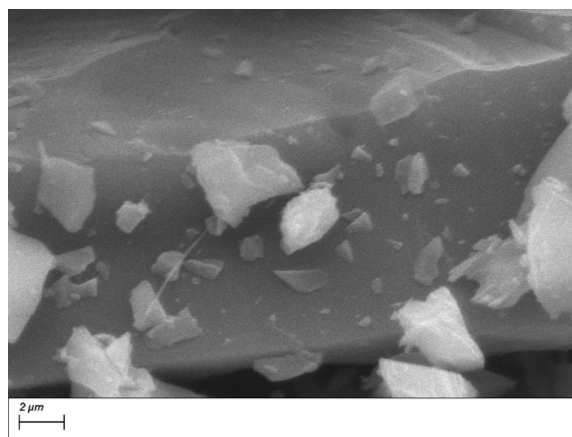


Figure 2: Scanning Electron Microscope (SEM) image of crystal milky quartz samples.

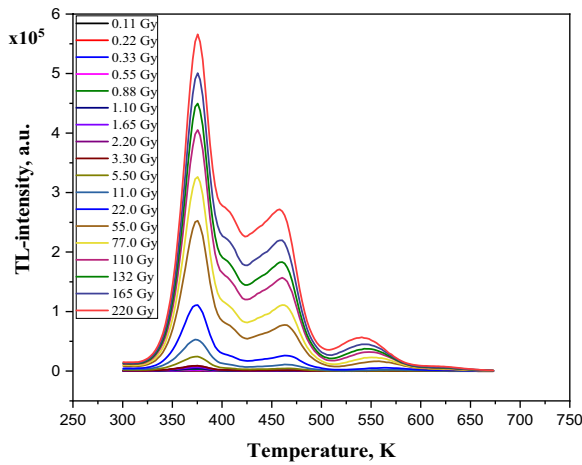


Figure 3: The glow curves at different doses ranging from 0.11 Gy to 220 Gy.

Kinetic analysis

The deconvolution analyses for the TL glow curves with the new designed TL software donated activation energies values of the different ten peaks with their corresponding frequency factors (Table 1). The best fit was tested by the Figure of Merit (FOM) [28] and determined frequency factor (*s*) from the general-order equation [29].

The frequency factor (*s*) can be obtained from the following equation:

$$s = \left(\frac{E\beta}{kT_M^2} \right) \frac{1}{1 + (b - 1) \left(\frac{2kT_M}{E} \right)} \exp \left(\frac{E}{kT_M} \right) \quad (1)$$

where β is the heating rate, *E* activation energy, T_M is the maximum temperature corresponding to the maximum intensity I_M , *k* is the Boltzmann constant, and *b* is the kinetic order.

In order to achieve the performance and obtaining a goodness of fitting, the figure of merit (FOM) is defined by:

$$FOM = \sum_{j_i}^{j_f} \frac{100(y_j - y(k_f))}{A} \quad (2)$$

where j_i and j_f represent the first and the last channel in the region of interest, respectively, y_j is the information content of channel, *j* and $y(k_f)$ is the value of the fitting function in channel (*j*). *A* is the integral value of the fitted glow curve at the region of interest.

$T_m - T_{stop}$ method

The $T_m - T_{stop}$ technique was applied to test the real number of peaks and their positions and to find the trap distributions in the examined quartz [30]. All samples prepared for this experiment

were annealed from room temperature up to 673 K for 1 h and followed by irradiation with 11 Gy to beta source. At First, a sample was heated to the stop temperature which began with a temperature of 323 K with a heating rate of 5 K/s. Then, the next sample was started from room temperature and ended in a selected stop temperature which has a small increment of 5 K with recording the thermoluminescence intensity of each step. Afterward, the same sample was measured again with the same heating rate in a temperature range from room temperature up to 673 K. The location of the first maximum in the second run was recorded as T_m . This procedure of measurement was repeated to have different stop temperatures (T_{stop}), and then T_m versus T_{stop} was plotted as shown in Fig. 5(a). Garlick and Gibson [31] supposed that for TL intensity, the maximum intensity at the initial part of the glow peak is not higher than 15%. The concentration of the trapped charge carriers $n(T)$ is constant and the TL intensity can be expressed as: $I = c \exp(-E/kT)$, where *c* is a constant and *k* is the Boltzmann constant, *E* is the activation energy (eV) and *T* is the absolute temperature. The plotting of $\ln(I)$ vs $1/kT$ (Arrhenius plot) yields a straight line and from its slope, the activation energy *E* can be obtained. The obtained activation energies are 0.663, 0.827, 1.05, 1.12, 1.43, 1.56, 1.62, 1.88, 2.51, and 2.86 eV at ten positions 312.42, 382.44, 405.97, 462.31, 470.61, 477.74, 502.05, 560.16, 568.94, and 602.73 K.

Various heating rates method

The various heating rates method is a method for measuring the shift of the maximum intensity of the glow peaks I_M and its corresponding temperature T_M at different heating rates. The VHR has the importance of being easy to apply when TL peaks are clearly isolated and it requires only I_M and T_M . However, if the TL glow peaks overlap, it can result in accurate values of the kinetic parameters. Chen and Winer [32] took the condition at the maximum intensity of the TL equations to determine the activation energy for first-, second-, and general-order TL peaks. In the case of general-order TL peaks, they have shown that the condition at maximum intensity could be written as:

$$\ln \left[I_M^{b-1} \left(\frac{T_M^2}{\beta} \right)^b \right] = \frac{E}{k} \frac{1}{T_M} + C \quad (3)$$

where *C* is a dimensionless constant, β is the heating rate, *E* is the activation energy, T_M is the maximum temperature corresponding to the maximum intensity I_M , *k* is the Boltzmann constant, and *b* is the kinetic order.

The plotting between $\ln \left[I_M^{b-1} \left(\frac{T_M^2}{\beta} \right)^b \right]$ and $1/T_M$ for every TL glow peak at each heating rate was represented as a straight line with slope of *E/k*, from which the activation energy can be calculated.

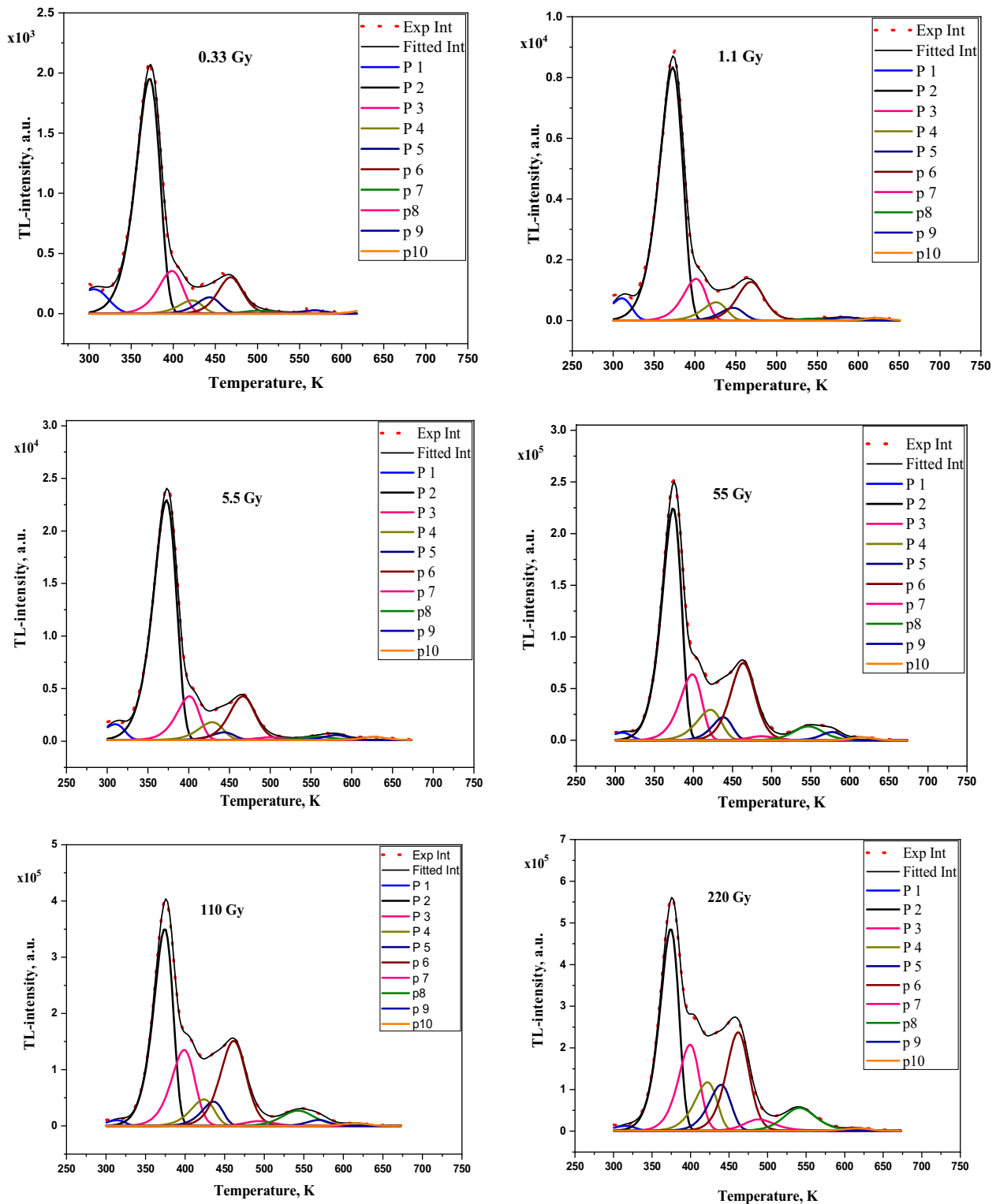


Figure 4: The glow curves of ten overlapping thermoluminescence peaks from four different doses (0.33, 1.1, 5.5, 55, 110, and 220 Gy) in the temperature range between 325 K and 650 K.

The VHR method was applied at different rates of 1, 2, 3, 5, 8, and 10 K.s⁻¹. These glow curves were deconvoluted using the CGCD method to separate the original TL glow peaks and to determine their kinetic parameters. The values of T_M , I_M ,

and b were obtained again by the VHR method. The relation between $\ln \left[I_M^{b-1} \left(\frac{T_M^2}{\beta} \right)^b \right]$ and $1/T_M$ can be plotted [as in Eq. 3] and the slope E/K of the obtained straight line estimates the

TABLE 1: Trapping parameters of the investigated samples by the new software.

Peak	T_m (k)	Activation energy (eV)	Order of kinetics (b)	Frequency factor (s^{-1})
P1	310.2±2.9	0.62±0.03	1.03±0.01	3.40×10 ¹⁰
P2	373.7±0.7	0.94±0.06	1.02±0.02	5.77×10 ¹²
P3	399.8±1.1	1.02±0.03	1.09±0.06	5.05×10 ¹²
P4	425.3±3.2	1.06±0.06	1.12±0.05	2.49×10 ¹²
P5	440.3±2.3	1.31±0.04	1.17±0.05	9.67×10 ¹⁴
P6	463.8±1.8	1.47±0.048	1.52±0.06	5.42×10 ¹⁵
P7	496.5±6.2	1.58±0.08	1.82±0.13	1.50×10 ¹⁶
P8	550.6±10.2	1.75±0.05	1.82±0.11	3.91×10 ¹⁵
P9	576.5±9.8	2.49±0.15	1.44±0.09	1.98×10 ²³
P10	622.8±8.6	2.95±0.16	1.59±0.03	2.32×10 ²⁵

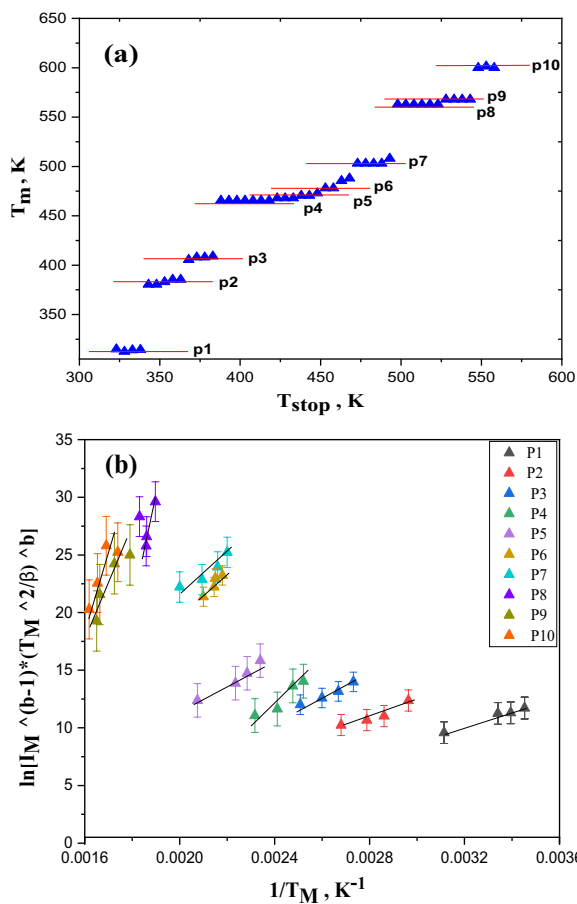


Figure 5: (a) $T_m - T_{stop}$ results of the investigated Egyptian quartz samples. (b) The plotting between $\ln \left[I_m^{b-1} \left(\frac{T_m^2}{\beta} \right)^b \right]$ and $1/T_m$ for each glow peak.

activation energy corresponding to the carrier traps [Fig. 5(b)].

The activation energies attained from the different methods of analysis, CGCD, $T_m - T_{stop}$, and various heating rates (VHR) are recorded in Table 2.

TABLE 2: The activation energies obtained using CGCD, $T_m - T_{stop}$ and VHR methods and the average value.

Peak	CGCD	$T_m - T_{stop}$	VHR	E (eV) average
P1	0.62	0.66	0.70	0.66±0.04
P2	0.94	0.83	0.84	0.87±0.06
P3	1.02	1.05	0.91	1.01±0.05
P4	1.06	1.12	1.12	1.10±0.04
P5	1.31	1.43	1.28	1.34±0.08
P6	1.47	1.56	1.35	1.46±0.10
P7	1.58	1.62	1.49	1.56±0.07
P8	1.76	1.86	1.64	1.75±0.11
P9	2.49	2.51	2.59	2.53±0.05
P10	2.96	2.86	2.98	2.93±0.07

Linearity

A necessary property for TL dosimeters is a linear direct correlation of the intensity of the glow curve with the applied dose over a certain dose range. This property indicates where the dosimeters under the investigation should be applied. The linearity behavior represents the response of the material to the applied doses of radiation. For this study, the investigated milky quartz samples were irradiated to different beta doses ranging from 2.2 Gy up to 220 Gy. Figure 6 shows the dose responses of all ten deconvoluted peaks of the investigated samples. Each peak has a different pattern which revealed different dose–response trends. Each deconvoluted peak represents a trap position with its kinetic order and kinetic parameters. The results revealed that P3, P5, P6, and P8 have a linear range from 2.2 to 220 Gy with R^2 of 0.983, 0.999, 0.987, and 0.992, respectively, and P7 have linearity from 2.2 to 110 Gy by R^2 0.979 then followed by supralinear trend up to 220 Gy by R^2 0.999, while P2, P4, and P10 have a similar trend of linearity from 2.2 to 110 Gy with R^2 of 0.981, 0.966, and 0.981, respectively. For P1 noticed the linearity range from 2.2 to 22 Gy by R^2 of 0.966 then exhibit exponential trend with R^2 of 0.989. Due to the variation of linearity trend for each peak, the investigated quartz samples can have different applications.

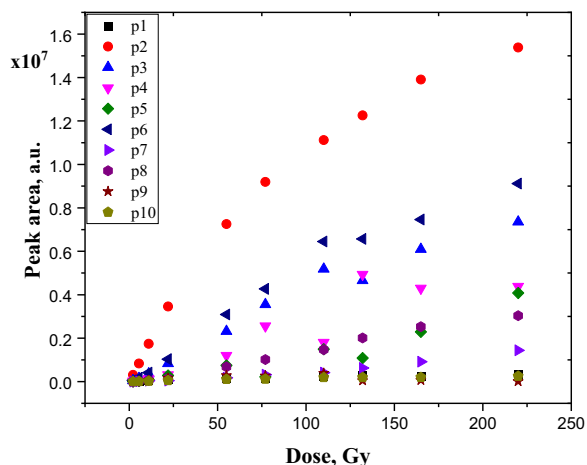


Figure 6: The TL response exhibited a linear behavior in the range from 2.2 Gy to 220 Gy in terms of a component resolved analysis.

The linearity index obtained by Furetta and Weng [33] which was described as:

$$f(D) = \frac{TL(D)/D}{TL(D1)/D1} \quad (4)$$

where D is the applied doses, $T(D)$ is the TL value corresponding to each D , $D1$ is the normalized dose in the linear part, and $T(D1)$ is the TL value corresponding to $D1$.

Minimum detectable dose (MDD)

McKeever et al. [34] described the minimum detectable dose (MDD) as the lowest detection limit or the threshold sense dose. The mean value of TL readings from a group of TL dosimeters after annealing and before the irradiation (B^*) adding to the double of the product of the standard deviation of these TL group of dosimeters ($2\sigma B$) and then multiplied by conversion factor F (which equals approximately 2.310 in units of mGy/nC). Furetta et al. [35] estimated the value of MDD by the following equation:

$$MDD = (B^* + 2\sigma B)F \quad (5)$$

The MDD for the investigated milky quartz samples was 24 μ Gy. This value is consistent with that of very low sensitivity results of the examined milky quartz samples.

Sensitivity

Sensitivity is the result of dividing the TL intensity by the product of the applied dose (in Gy) and the mass of the sample (in mg). Figure 7(a) represents the linearity by the total area under the glow curve. The linearity revealed two ranges: the first one is a linear dose response from 0.11 Gy to 22 Gy and the second one is a supralinear trend after applying doses from 22 Gy up to 220 Gy. Figure 7(b) represents the sensitivity, which changed according to the range of applied dose. By increasing the applied

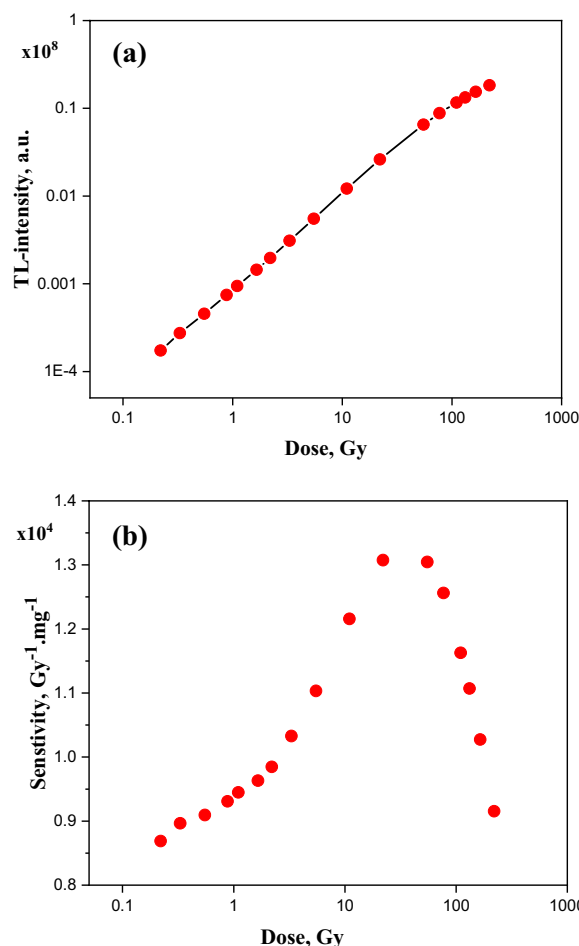


Figure 7: The linear behavior in the range from 0.11 Gy to 22 Gy and supralinear range from 22 to 220 Gy in terms of (a) the total area under the glow curve, and (b) the sensitivity of the Egyptian milky quartz samples in the linear range (22 mGy to 22 Gy) and supralinear range (22 Gy to 220 Gy) curve.

dose to be in the range (0.11–22 Gy), the sensitivity increases then decreases during supralinear range. This can be explained by the change in the attitude of the linearity curve.

Fading

The fading signal measures the possibility of undesirable escaping electrons from the traps between irradiation and measurements. For measuring the fading parameter to our examined samples, the samples were exposed to 11 Gy to beta source and were stored inside black boxes to avoided the optical fading at room temperature for different storage times 0, 1, 3, 7, 15, 20, and 30 days. It was observed from Fig. 8 that the whole glow curve reduced to about 80% from its original value after 1 day then to about 20% from the remaining signal after 3 days. From 7 days up to 15 days, the TL signal is faded by very small amount about 6% then reduced to about 49% from the remained signal after 20 and 30 days.

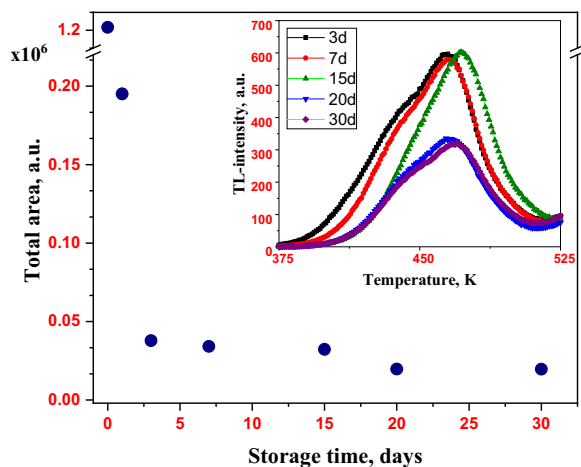


Figure 8: The relation between TL intensity of glow curve to the Egyptian milky quartz samples with different storage times.

Conclusions

The present study examined the TL properties of milky quartz associated with Metamorphic Rocks in Eastern Desert, Egypt. The kinetic analysis of the glow curve shows that there were ten trapping sites. The linearity of the investigated sample was examined for each component of the glow curve. The analysis of the glow curve was studied also by $T_m - T_{stop}$ and various heating rates (VHR) giving the kinetics parameters (activation energy E , eV). The minimum detectable dose (MDD) of the investigated quartz samples was calculated. The dosimeter had good reproducibility. Fading signal was examined for different storage times.

In future, the research group will investigate the TL characteristics of the other types of milky quartz extracted from Egypt. Due to the high sensitivity and good reproducibility of the examined samples and their wide-ranging of linearity, the authors recommend that the investigated quartz is used in radiation dosimetry.

Experimental and materials

The investigated samples of milky quartz associated with metamorphic rocks were collected from Gebel Rod El Barram Eastern Desert of Egypt at Lat. $25^{\circ} 05' 56''$ N and Long $34^{\circ} 04' 10''$ E. The samples associated with Talc-Schist and the Tectonostratigraphic Unit were Infrastructural rocks.

The Egyptian milky quartz samples were cleaned and washed with distilled water. Then they were cut into square disks of $5\text{ mm} \times 5\text{ mm}$ and 1 mm thick. The TL glow curves recorded at temperature from 323 to 673 K with heating rate of 5 K/s using Lexsyg Smart TL/OSL luminescent reader. The reader is controlled by LexStudio 2.0 operating software on a personal computer. The reader has a built-in source of $^{90}\text{S}/^{90}\text{Y}$, with a dose rate of 0.11 Gy/s, which emits beta particles with a maximum energy

of 2.2 MeV. The reader has also bi-alkaline cathode photomultiplier tube (Hamamatsu) and it was connected to a nitrogen supply for cooling. The readings were taken using the filter IRSL/TL—wideband blue. The attained glow curves of the samples were deconvoluted using new TL software [36] designed in the Lab of Nuclear Radiation Measurements in the Department of Physics, Faculty of Science, Ain Shams University, Cairo, Egypt. The TL glow curve deconvolution performed by optimization algorithms through the following steps. First, the user chooses the fitting algorithm. Second, the user determines the number of peaks. Third, the user explodes the algorithm with an initial guess of each peak parameters. The optimization algorithms stopped when reached specific accuracy by varying the optimization parameters regardless of whether the resultant final parameters have physically acceptable values or not. Therefore, the user is given the opportunity of fixing some parameters if the solver fails to get acceptable physical parameters [36]. The investigated samples were annealed by first heating up to 673 K for 1 h, and then slowly cooling down. The annealing is done by an electrical furnace Nabertherm model (D-2804 lilitenthal/Bremen-w.-Germany). The samples were irradiated to various doses ranging from 0.11 Gy up to 220 Gy. The sensitivity of the samples has no change for the repeating process which was examined by irradiating them to a certain dose (11 Gy) five times under the same experimental conditions.

The crystallinity of the investigated quartz samples was examined by X-ray diffraction (XRD). The powdered sample was examined by XRD analysis using a PHILIPS® X'Pert Multi-Purpose Diffractometer with Cu anode of wavelength (λ) = 1.54056 Å and operating at 40 kV and 30 mA. The data were collected for (2θ) range from 10° to 80° .

The elemental analysis for the Examined quartz samples was performed using atomic absorption spectrometer, manufactured in Germany. The samples were digested in acid (HNO_3 and HF) of silicon dioxide in a closed vessel using a pressure-controlled microwave to determine the metal contents by spectroscopy methods.

Funding

Open access funding provided by The Science, Technology & Innovation Funding Authority (STDF) in cooperation with The Egyptian Knowledge Bank (EKB).

Data availability

The data are available on request.

Declarations

Conflict of interest The authors declare that they have no conflict of interest.

Open Access

This article is licensed under a Creative Commons Attribution 4.0 International License, which permits use, sharing, adaptation, distribution and reproduction in any medium or format, as long as you give appropriate credit to the original author(s) and the source, provide a link to the Creative Commons licence, and indicate if changes were made. The images or other third party material in this article are included in the article's Creative Commons licence, unless indicated otherwise in a credit line to the material. If material is not included in the article's Creative Commons licence and your intended use is not permitted by statutory regulation or exceeds the permitted use, you will need to obtain permission directly from the copyright holder. To view a copy of this licence, visit <http://creativecommons.org/licenses/by/4.0/>.

References

- J. Götze, *Miner. Mag.* **73**, 645 (2009). <https://doi.org/10.1180/minmag.2009.073.4.645>
- P.J. Heany, C.T. Prewitt, G.V. Gibbs, *Mineral. Soc. Am.* **29**, 606 (1994). <https://doi.org/10.1515/9781501509698>
- F. Pirajno, *Hydrothermal Mineral Deposits: Principles and Fundamental Concepts for the Exploration Geologist* (Springer, Dordrecht, 2009). <https://doi.org/10.1007/978-1-4020-8613-7>
- U. Heynke, O. Leeder, H. Schulz, *Miner. Petrol.* **46**, 315 (1992). <https://doi.org/10.1007/BF01173570>
- M. Ezz-El Din, A.M. Abouzeid, K.H. El Maadawy, A.M. Khalid, R.E. El Sherif, *J. Min.* **5**, 9 (2016) <https://doi.org/10.14355/mwe.2016.05.002>
- S. El-Gaby, F.K. List, R. Tehrani, *The Geology of Egypt* (Balkema, Rotterdam, 1990), p. 175. <https://doi.org/10.1201/9780203736678>
- M.A. Hassan, A.H. Hashad, *The Geology of Egypt* (Balkema, Rotterdam, 1990), p. 201. <https://doi.org/10.1201/9780203736678>
- M.Z. El-Bialy, *The Geology of Egypt* (Springer, Switzerland, 2020). https://doi.org/10.1007/978-3-030-15265-9_2
- K.A. Ali, A. Andresen, R.J. Stern, W.I. Manton, S.A. Omar, A.E. Maurice, *Geol. Mag.* **149**, 783 (2012). <https://doi.org/10.1017/S0016756811000975>
- A.M. Lundmark, A. Andresen, M.A. Hassan, L.E. Augland, M.A.A. El-Ru, G.Y. Boghdady, *Gondwana Res.* **22**, 227 (2012) <https://doi.org/10.1016/j.gr.2011.08.017>
- Z. Hamimi, M.A. Abd El-Wahed, H.A. Gahlan, S.Z. Kamh, *The Geology of the Arab World—An Overview* (Springer, Berlin, 2019). https://doi.org/10.1007/978-3-319-96794-3_1
- G. Polymeris, G. Kitis, V. Pagonis, *Radiat. Meas.* **41**, 554 (2006). <https://doi.org/10.1016/j.radmeas.2006.03.006>
- R. Zhou, M. Wei, B. Song, Y. Zhang, Q. Zhao, Li.T. Pan *B Nucl. Instrum. Meth. B* **375**, 32 (2016) <https://doi.org/10.1016/j.nimb.2016.02.067>
- C. Furetta, World Sci. Singapore (2003). <https://doi.org/10.1142/5167>
- V. Pagonis, G. Kitis, C. Furetta, *Numerical and Practical Exercises in Thermoluminescence* (Springer, New York, 2006)
- R. Chen, S. McKeever, *Theory of Thermoluminescence and Related Phenomena* (World Science Publishing Co. PVT. Ltd., Singapore, 1997)
- M. Sabry, H.A. Alazab, A. Gad, N. El-Faramawy, *J. Lumin.* **238**, 118273 (2021). <https://doi.org/10.1016/j.jlumin.2021.118273>
- N. El-Faramawy, H.A. Alazab, A. Gad, M. Sabry, *Radiat. Phys. Chem.* **190**, 109793 (2022). <https://doi.org/10.1016/j.radphyschem.2021.109793>
- S. Riedesel, A.M.T. Bell, G.A.T. Duller, A.A. Finch, M. Jain, G.E. King, N.J. Pearce, H.M. Roberts, *Radiat. Meas.* **141**, 106541 (2021). <https://doi.org/10.1016/j.radmeas.2021.106541>
- G.P.S. Silva, M.C.S. Nunes, C. Ulsen, R. Künzel, E.M. Yoshimura, N.M. Trindade, *J. Lumin.* **213**, 117802 (2021). <https://doi.org/10.1016/j.jlumin.2020.117802>
- J.M. Kalita, Ş Kaya-Keleş, G.Ö. Çakal, N. Meriç, *J. Lumin.* **230**, 117759 (2021). <https://doi.org/10.1016/j.jlumin.2020.117759>
- S. Akça-Özalp, Z.G. Portakal-Uçar, M. Oğlakçı, M. Yüksel, Y.Z. Halefoğlu, M. Topaksu, *J. Lumin.* **240**, 118427 (2021). <https://doi.org/10.1016/j.jlumin.2021.118427>
- A.S. Murray, A.G. Wintle, *Radiat. Meas.* **29**, 65 (1998). [https://doi.org/10.1016/S1350-4487\(97\)00207-2](https://doi.org/10.1016/S1350-4487(97)00207-2)
- J.F. De Lima, M.S. Navarro, M.E.G. Valerio, *Radiat. Meas.* **35**, 155 (2002). [https://doi.org/10.1016/S1350-4487\(01\)00283-9](https://doi.org/10.1016/S1350-4487(01)00283-9)
- G. Kitis, V. Pagonis, H. Carty, E. Tatsis, *Rad. Prot. Dosim.* **100**, 225 (2002). <https://doi.org/10.1093/oxfordjournals.rpd.a005852>
- S. Farouk, H. El-Azab, A. Gad, H. El-Nashar, N. El-Faramawy, *Lumin.* **35**, 586 (2020). <https://doi.org/10.1002/bio.3760>
- S. Farouk, A. Gad, H. El-Azab, H. El-Nashar, N. El-Faramawy, *Radiat. Phys. Chem.* **181**, 109333 (2021). <https://doi.org/10.1016/j.radphyschem.2020.109333>
- M. El-Kinawy, H. El-Nashar, N. El-Faramawy, *S.N. Appl. Sci.* **1**, 834 (2019). <https://doi.org/10.1007/s42452-019-0876-7>
- H.G. Balian, N.W. Eddy, *Nucl. Instrum. Meth.* **145**, 389 (1977). [https://doi.org/10.1016/0029-554X\(77\)90437-2](https://doi.org/10.1016/0029-554X(77)90437-2)
- C.E. May, J.A. Partridge, *J. Chem.* **40**, 1401 (1964). <https://doi.org/10.1063/1.1725324>
- S.W.S. McKeever, *Nucl. Instr. Meth.* **175**, 19 (1980). [https://doi.org/10.1016/0029-554X\(80\)90238-4](https://doi.org/10.1016/0029-554X(80)90238-4)
- G.F.J. Garlick, A.F. Gibson, *Proc. Phys. Soc. Lond.* **60**, 574 (1948). <https://doi.org/10.1088/0959-5309/60/6/308>
- R. Chen, S.A.A. Winer, *J. Appl. Phys.* **41**, 5227 (1970). <https://doi.org/10.1063/1.1658652>
- C. Furetta, P.S. Weng, *Operational Thermoluminescence Dosimetry* (World Scientific, Singapore, 1998)
- S.W. McKeever, M. Moscovitch, P.D. Townsend, *Nucl. Tech.* (1995)
- C. Furetta, M. Porkic, R. Salamon, G. Kitis, *Appl. Radiat. Isot.* **52**, 243 (2000). <https://doi.org/10.1016/S0969-8043>

Publisher's Note Springer Nature remains neutral with regard to jurisdictional claims in published maps and institutional affiliations.